# Molecular dynamics calculations suggest a conduction mechanism for the M2 proton channel from influenza A virus

Ekta Khurana[a,b,1], Matteo Dal Peraro[a,c,1], Russell DeVane[a], Satyavani Vemparala[d], William F. DeGrado[a,e,1], and Michael L. Klein[a]

[a]Department of Chemistry, University of Pennsylvania, Philadelphia, PA 19104-6323; [b]Department of Molecular Biophysics and Biochemistry, Yale University, New Haven, CT 06520; [c]Laboratory for Biomolecular Modeling, Institute of Bioengineering, School of Life Sciences, Ecole Polytechnique Fédérale de Lausanne (EPFL), CH-1015 Lausanne, Switzerland; [d]The Institute of Mathematical Sciences, Chennai, 600 041 India; and [e]Department of Biochemistry and Biophysics, School of Medicine, University of Pennsylvania, Philadelphia, PA 19104-6059

Contributed by William F. DeGrado, November 21, 2008 (sent for review May 20, 2008)

**The M2 protein of the influenza A virus is activated by low endosomal pH and performs the essential function of proton transfer into the viral interior. The resulting decrease in pH within the virion is essential for the uncoating and further replication of the viral genetic material. The x-ray crystal [Stouffer AL, *et al.* (2008) Nature 451:596–599] and solution NMR [Schnell JR, Chou JJ (2008) Nature 451:591–595] structures of the transmembrane region of the M2 homo-tetrameric bundle both revealed pores with narrow constrictions at one end, leaving a question as to how protons enter the channel. His-37, which is essential for proton-gating and selective conduction of protons, lies in the pore of the crystallographic and NMR structures. Here, we explore the different protonation states of the His-37 residues of the M2 bundle in a bilayer using molecular dynamics (MD) simulations. When the His-37 residues are neutral, the protein prefers an $Open_{out}$-$Closed_{in}$ conformation in which the channel is open to the environment on the outside of the virus but closed to the interior environment of the virus. Diffusion of protons into the channel from the outside of the virus and protonation of His-37 residues in the tetramer stabilizes an oppositely gated $Closed_{out}$-$Open_{in}$ conformation. Thus, protons might be conducted through a transporter-like mechanism, in which the protein alternates between $Open_{out}$-$Closed_{in}$ and $Closed_{out}$-$Open_{in}$ conformations, and His-37 is protonated/deprotonated during each turnover. The transporter-like mechanism is consistent with the known properties of the M2 bundle, including its relatively low rate of proton flux and its strong rectifying behavior.**

ion channel | transporter | pH activated | His gate | simulations

The M2 protein from the influenza A virus is commonly described as a pH-activated proton channel based on its function of transferring protons into a virus. After endocytosis of the virus, the low pH in the endosome activates the channel. The transfer of protons to the viral interior via the M2 protein permits the uncoating of the viral RNA and fusion of the viral envelope with the endosomal bilayer, an important step in the life cycle of the virus (1). The M2 protein is a homotetramer, with each monomer consisting of a 24-residue N-terminal extracellular domain, a transmembrane (TM) domain of 19 residues, and a 54-residue cytoplasmic domain. A 25-residue TM segment: residues 22–46 (called M2-TM hereafter) spans the hydrophobic region of the membrane, and includes a few hydrophilic residues on either end. M2-TM forms tetrameric bundles (with the four chains referred to as A– D hereafter) and binds adamantane-containing drugs as the full M2 protein does, both in micelles (2) and in lipid bilayers (3–6).

Experimentally based model structures of M2-TM have been available for some time (4–9) and have been computationally investigated by several authors (10–18); however, high-resolution structures have only recently been determined. Schnell and Chou have reported an NMR structural ensemble for the peptide, spanning residues 18–60 in detergent micelles at high pH (19). Stouffer *et al.*, however, have used x-ray diffraction to solve the structures of M2-TM: crystallized under neutral and low pH conditions (20). Importantly, solid-state NMR studies of the helix-spanning region of the channel (in bilayers that most closely resemble a native membrane) have provided high-resolution measurements of individual helical distances and orientations: these data are in agreement with the crystallographic and solution NMR structures (8, 9).

The flux of protons through the M2 protein increases as the pH is lowered, which is a result of the increase in the permeant ion concentration and a "gating" process that involves His-37 and Trp-41 residues (which line the pore of M2-TM near the C terminus) (21). The x-ray crystal structure of the channel, solved at low pH in the presence of the channel-blocking drug amantadine, is closed near the N terminus but open in the vicinity of His-37 and Trp-41. The NMR structure, however, is completely occluded at the C terminus, and has only a very small opening near the N terminus. Surprisingly, the crystallographic structure determined for M2-TM (crystallized near neutral pH and in the absence of channel-blocking drugs) has hybrid characteristics: The N-terminal half of the structure possesses fourfold rotational symmetry, with the channel pore very constricted near Val-27. In contrast, the C-terminal half of the structure exhibits some asymmetry; one of the four helices (chain D) shows a slight bend near the middle of the TM region centered on Gly-34. This bend allows aromatic interactions between Trp-41 on chain D and His-37 on chain C, and a salt bridge between Arg-45 of chain D and Asp-44 of chain C. The latter not observed in the other subunits, may be a reflection of the mixed protonation state of the His-37 tetrad; a scenario that could arise because the structure was crystallized at a pH that falls between the $pK_a$ values of the His-37 residues in the tetramer (4). Based on this hypothesis, a family of fully symmetric structures was created from each of the monomers (A–D). The tetrameric bundles obtained from subunits A– C (designated A4 through C4) are very similar in structure to the low pH crystallographic structure. The D4 bundle resembles the NMR structure, being closed at both the N terminus and the C terminus (Fig. 1).

One particularly interesting question arises from these structural studies: how might a proton enter the channel? Whereas

Author contributions: E.K., M.D.P., W.F.D., and M.L.K. designed research; E.K., M.D.P., and R.D. performed research; E.K., M.D.P., R.D., and S.V. analyzed data; and E.K., M.D.P., W.F.D., and M.L.K. wrote the paper.

Conflict of interest statement: This work was supported by InfluMedix. W.F.D. and M.L.K. are founders and members of the Scientific Advisory Board of InfluMedix.

Freely available online through the PNAS open access option.

[1]To whom correspondence may be addressed. E-mail: ekta.khurana@yale.edu, matteo.dalperaro@epfl.ch, or wdegrado@mail.med.upenn.edu.

© 2009 by The National Academy of Sciences of the USA

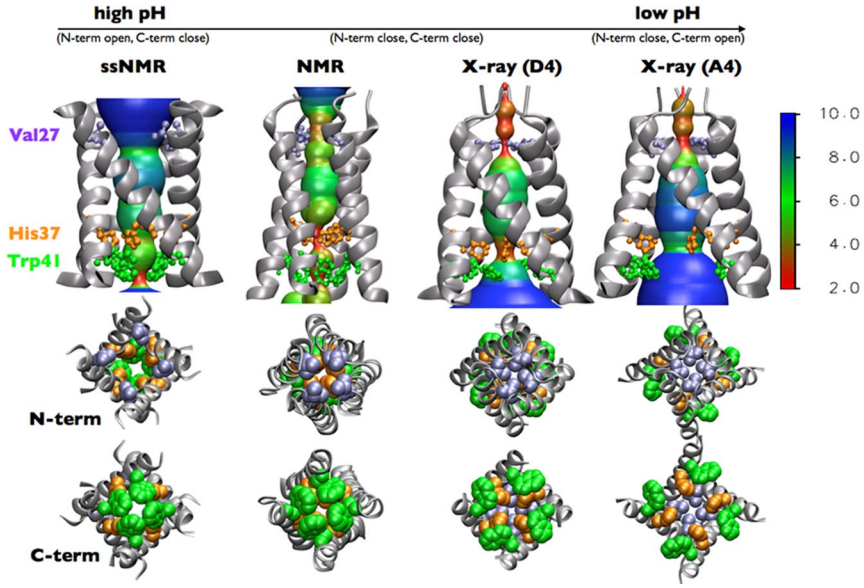


**Fig. 1.** Structures of M2-TM. Left to right: ssNMR, solid state NMR structure (3). NMR, solution NMR structure (19). x-ray (D4), D4 model derived by replication of chain D of crystallographic structure (20). x-ray (A4), A4 model derived by replication of chain A of crystallographic structure (20). The HOLE profiles (40) (color coding scale in Å on the right), both N-terminal and C-terminal views are shown. Relevant pore lining residues are shown as VDW spheres: Val-27 (ice blue), His-37 (orange), and Trp-41 (green).

the N-terminal region of the pore surrounding Val-27 is almost completely occluded in the solution NMR (19) and crystallographic structures (20), with diameters of 3.1 Å and 1.5 Å, respectively, previous work has suggested a much greater opening; one model of this type of structure (proposed by Cross and coworkers) (3) is shown in Fig. 1. Thus, it is possible that conformational changes facilitate proton transfer through the N-terminal region of the pore, although the connection between such transitions and the protonation state of His-37 (as well as its significance in the overall conduction mechanism) remains elusive. Any resolution of this issue must be consistent with essential electrophysiological properties of the channel, which include a very low rate of proton flux ($<10^4$ protons per second) relative to classic ion channels (22), an intermediate solvent isotope effect, and very strong rectification [the channel allows rapid diffusion of protons down their concentration gradient when the outside is at low pH and the inside is at high pH, but it does not allow efficient proton flux when the inside is at low pH and the outside is at high pH (21–23)].

We describe molecular dynamics (MD) simulations of the crystal structure, by using the crystal structure (PDB id: 3BKD) of the amantadine-free channel at 2.0-Å resolution (20) as the starting configuration. In parallel, the crystallographically defined D4 model was also examined, by using different protonation states of the His-37 tetrad to mimic the pH drop within the endosome (4). The results suggest that the channel behaves as a pH-dependent transporter, switching between a state in which the N-terminal end is open to the exterior of the virus and the C terminus is closed to the interior and an oppositely gated form.

## Results and Discussion

The only ionizable groups in the channel cavity are the four His-37 residues; channel conduction depends on their protonation states (4). In the pH range relevant for M2 proton conductivity (≈5 to 7), the protonation/deprotonation of the His-37 residues is likely to be rate-limiting and on the ms-to-sec time-scale (21–23): slower than the timescale accessible to current MD simulations. Therefore, we eliminated the slow chemical steps of protonation/deprotontation, and used MD simulations of approximately 30 ns to explore the structural relaxations following these events. The resulting ensemble provides a picture of how the structural and dynamic properties of the protein change in response to pH.

**Simulation of the Crystallographic Structure in the Tetra-Protonated State.** Simulation of the experimentally observed crystal structure with four His-37 charged (crystal-4) in a DMPC bilayer was performed. The RMSD of the protein backbone stabilizes within the 30-ns simulation at 2.9 (4) Å. The extraviral entrance to the pore stays constricted at the N-terminal Val-27 gate (≈2 Å) close to the initial value of approximately 1.5 Å. The very narrow Val-27 gate limits transfer of water into the channel, which occurs via transient single files. During the last 8 ns of the simulation, only six water molecules pass the narrow Val-27 gate.

His-37 and Trp-41 are located toward the C-terminal end of the pore, near the inside of the virus. The cavity surrounding these residues becomes well solvated in the simulation. The pore around the solvated His-37 tetrad is slightly wider for the crystal-4 simulation (≈7.5 Å), compared with the initial crystal structure (5 Å) (Figs. 1 and 2), but similar to the crystal structure of M2 at lower pH. The aromatic interactions between His-37 of

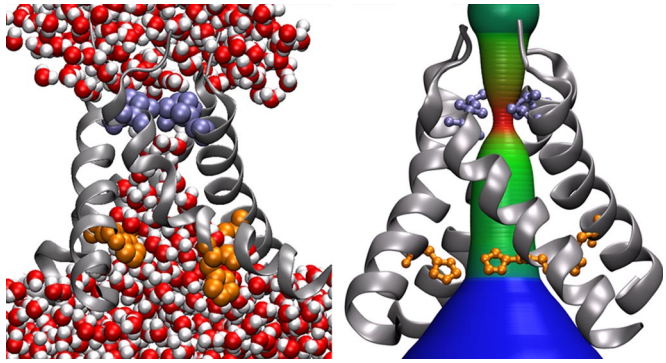

**Fig. 2.** Low pH state. Snapshot from crystal-4 MD simulation at $t = 30$ ns and the MD averaged pore profile computed over the last 4 ns. Val-27 (ice blue) and His-37 (orange) gates are shown.

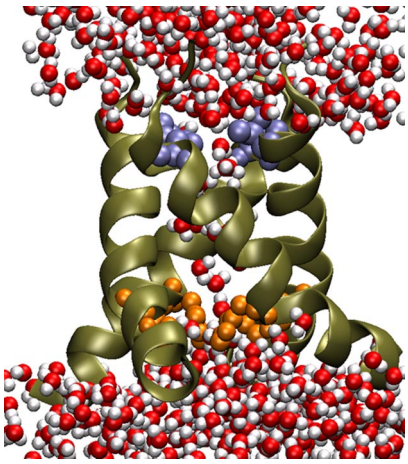

**Fig. 3.** High pH state. Water accessibility at the N-terminal from a snapshot of D4–0 simulation at $t = 30$ ns with Val-27 (iceblue) and His-37 (orange) gates. Water molecules can easily go through the open Val 27 gate as seen in the figure.

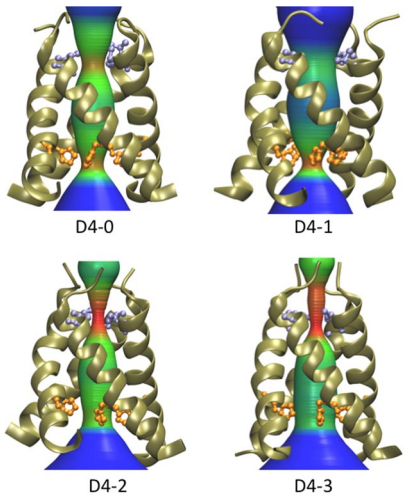


**Fig. 4.** High-to-low pH transition. Pore diameters averaged over the last 4 ns of trajectories along the length of the pore (color coding scale in Fig. 1). Positions of Val-27 (ice blue) and His-37 (orange) gates are shown.

chain C and Trp-41 of chain D found in the crystal structure likely correspond to a lower protonation state than the tetra-protonated form simulated here. As expected, these interactions are lost in the simulation thereby leading to a more symmetric conformation of the C-terminal domain. In summary, the simulation suggests that protonation of all four His-37 residues favors a $Closed_{out}$-$Open_{in}$ conformation; in this state the constricted N-terminal region of the pore presents a kinetic barrier to the entry of water and protons into the channel from the outside of the virus, whereas the dilation of the C-terminal region facilitates diffusion of protons and water from the inside of the virus in and out of this region of the channel.

**Low Degrees of Protonation Favor an $Open_{out}$-$Closed_{in}$ Conformation.** Simulations of the D4 bundle with all neutral His-37 (D4–0 model) and one charged His-37 (D4–1 model) reflect the resting state of the channel at high pH. These protonation states also reflect possible intermediates in a conduction mechanism in which protonation/deprotonation of the individual His residues occurs during proton translocation. The starting "D4" model (20) of the channel was constructed by replication of chain D of the protein crystallized at intermediate pH. This structure, which is closed at the C terminus was proposed to be progressively favored as the number of protons on His-37 residues are reduced. The His-37-Trp-41 interaction that is evident between chains C and D in the crystal structure is present at all of the interfaces in the symmetric D4 bundle. Furthermore, the regions around both the Val-27 and His-37 residues are very constricted with pore diameters of approximately 1 Å and 3 Å, respectively (Fig. 1).

The RMSD of the protein backbone settles within a timescale of approximately 20 ns at 2.2 (4) Å for the D4–0 simulation and at 2.4 (5) Å for D4–1. The pore diameter of approximately 3 Å at the His-37 gate is conserved for both the D4–0 and D4–1 simulations, whereas the Val-27 gate opens significantly (Figs. 3 and 4). Interestingly, the pore diameter around the Val-27 gate for the D4–0 simulation (≈3.6 Å) is close to the value observed in the solution NMR structure of the protein (3.1 Å) (Fig. 1) (19). This region is wider in the case of D4–1 (≈6.9 Å). It is interesting to note that water molecules can easily pass through the gate in both the simulations (Fig. 3). The His-37/Trp-41′ interactions, which clamp the internal end of the channel in a closed conformation in the starting D4 simulation, are retained throughout the simulation. The center of mass distances for His-37 and Trp-41 of neighboring helices remain close to the initial value of 5.6 Å for the entire trajectories of D4–0 and D4–1.

In summary, this set of MD simulations indicates that when the protonation of the His residues is low, the protein adopts an $Open_{out}$-$Closed_{in}$ conformation. It is noted that although the pore diameter of His-37 gate is approximately 3 Å in the D4 model, and shows some permeability to water, it is even narrower in the high-pH solution NMR structure (19). Such a narrow His-37 gate would show extremely little permeability to water. The His-37/Trp-41′ interactions stabilize the narrow C terminus. The Trp-41 residue plays an important role in this interaction, because it impedes access of water (and presumably protons) on the inside of the virus to His-37. However, the N terminus region widens, significantly increasing the diffusion of water and protons into the central region of the pore. Thus, in the $Open_{out}$-$Closed_{in}$ conformation His-37 has greater kinetic access to protons on the outside than it does to protons on the inside of the virus.

**High Degrees of Protonation Favor a $Closed_{out}$-$Open_{in}$ Conformation.** Simulations of the D4 bundle with doubly (D4–2 model) and triply (D4–3 model) charged His-37 gave rise to a $Closed_{out}$-$Open_{in}$ conformation, very similar to that observed when the crystal structure was simulated in the tetra-protonated state (Fig. 2). In these simulations, the His-37 gate widens relative to the initial D4 bundle structure, whereas the Val-27 gate stays very constricted with a pore diameter of approximately 2 Å (Fig. 4). The increased charge resulting from the protonated His-37 residues in the D4–2 and D4–3 simulations leads to a greater degree of hydration, facilitating the increase in pore radii in the vicinity of His-37. Concomitantly, the tight hydrophobic interaction around the Val-27 gate is stabilized relative to the D4–0 and D4–1 simulations. As the His-37 gate opens, the His37/Trp41′ interactions at the helix interfaces are lost. Consistent with this observation, the RMSD of the protein backbone gradually diverges upon increase in the protonation state of the His-37 tetrad, with respect to the initial D4 bundle model [D4–0: 2.2 (4) Å, D4–1: 2.4 (5) Å, D4–2: 2.6 (3) Å, and D4–3: 3.2 (3) Å].

**Implications for the Mechanism of Proton Conduction.** Before discussing the implications of these simulations to the mechanism of conduction, it is important to consider the underlying assumptions and the potential limitations of these calculations.

The slow steps in proton conduction are likely to be associated with protonation/deprotonation. As discussed previously (22), if His-37 is protonated at a rate of $10^8$ to $10^{10}$ $M^{-1}sec^{-1}$, dissociation will occur at a rate of $10^0$ to $10^4$ $sec^{-1}$ (for the His-37 residues which have $pK_a$'s in the range of 6 to 8) (4, 24). These rates are within the range estimated for the conduction of M2 under physiological conditions in transfected cells (22). Here, MD is used to map subsequent conformational changes by exploring the structural perturbations associated with the change in protonation state. We began by simulating an asymmetric conformation, which appeared, in the crystallographic structure, to be in an intermediate charged state. When this structure was fully protonated on each of the His-37 residues, the simulations rapidly converged on a structure strongly resembling the crystallographic structure solved for a form of the peptide crystallized at low pH. Thus, this simulation is in good agreement with experimental data.

We next performed simulations of the D4 structure, which is a model for the neutral form of the channel (created by applying symmetry to one of the crystallographic monomers of the asymmetric crystal structure). As expected, in the D4–0 and D4–1 calculations, the conformation is relatively stable, maintaining His-37/Trp-41′ interactions anticipated to be important for stability. An interesting feature of these calculations is that the Val-27 sphincter frequently adopts a configuration that is more open than it had appeared in the original model. Indeed, the size of the sphincter in the D4–0 state is similar to that observed in a high-pH solution NMR structure of the protein (19), concurring once again with experimental results. Along these lines, it is interesting to note that Zhou and coworkers observed a similar fluctuating constriction at Val-27 in a very recent MD simulation of M2-TM with one of the four His-37 residues protonated (18). In this simulation the sphincter defined by Val-27 fluctuated between a state with a diameter of approximately 2.0–3.0 Å that was able to support a single-file column of water, and a completely closed conformation [Fig. 2 *A–D* of (18)]; the two conformations fluctuated on the ps/ns time scale and had approximately equal probabilities [Fig. 1 of (18)]. Although different starting structures were used in this simulation of Zhou and coworkers, the size and fluctuations of the Val-27 sphincter are nevertheless similar to those observed in the present simulation of the neutral form of the channel. It is interesting to note that in our simulations, the Val-27 sphincter opened even more in the singly protonated D4–1 simulation. However, we have conducted only a single simulation of this state, so are unable to extrapolate conclusively from this observation.

With increasing protonation of the doubly, triply, and quadruply charged states, the Val-27 sphincter constricts; concomitantly, the pore opens near residues His-37 and Trp-41. An abrupt switch from an $Open_{out}$-$Closed_{in}$ to a $Closed_{out}$-$Open_{in}$ conformation occurs when the channel reaches the doubly protonated state. The $Closed_{out}$-$Open_{in}$ conformation allows more efficient solvation of the charged His residues and minimization of their electrostatic repulsions. However, it is likely that these repulsive interactions are over-estimated for the +2 state, because the force field used in these simulations does not adequately represent nonclassical interactions associated with proton tunneling and low-barrier hydrogen bonds - factors that appear to help stabilize the doubly charged species (4). Thus, although our simulations show a clear trend toward greater opening of the channel as protons accumulate on His-37, it is likely that they underestimate the stability of the $Open_{out}$-$Closed_{in}$ states when the protein is at intermediate charged states.

There are two possible conductance mechanisms of the M2 protein. One view is that M2 is a classical gated channel, in which protonation of His-37 opens a continuous water-filled pore containing a chain of hydrogen-bonded water molecules that mediate rapid proton transfer (17, 22). Given the low conductance of the channel, this mechanism has been modified to suggest that the probability of occurrence of a single-file chain of water molecules is very low at any given time, even when the channel is gated "on" (18). However, as discussed (22), a gated channel model does not explain the fact that the chord conductance saturates at low pH (24) even as the concentration of the permeant ion increases. Also, it is not clear how this mechanism accounts for the rectification and other unusual conduction properties of the channel. Alternatively, Pinto and coworkers (7) proposed that His-37 is directly involved in conduction, being protonated/deprotonated with each transit of a proton. The current studies are most consistent with this hypothesis, providing a structural and dynamic framework to this permeation model.

The most important mechanistic insights gained from these calculations are: 1) M2-TM exists essentially in two different states: open at one or the other end of the pore (rarely at both ends); 2) the $Open_{out}$-$Closed_{in}$ state has a small, fluctuating opening near the N terminus and a C terminus that is clamped shut by interhelical interactions involving His-37/Trp-41′ and Asp-44/Arg-45′; 3) the $Closed_{out}$-$Open_{in}$ state has a more tightly closed N-terminal region and a fluctuating opening near the C terminus; and 4) the populations of these two ensembles depend on the protonation state of the His-37 residues—interconversion between the two ensembles occurs in 10–20 ns time scale. Fig. 5 illustrates a schematic model for the conduction cycle of M2. Although more complex mechanisms are possible, we assume that the primary conduction mechanism involves cycling between protonation states with a net difference of a single proton (probably corresponding to a tetramer with two vs. three protonated His-37 residues). In the $Open_{out}$-$Closed_{in}$ conformation, His-37 is exposed only tothe outside pH ($pH_{out}$) and it cannot be easily protonated from the inside of the virus, whereas the opposite holds for the $Closed_{out}$-$Open_{in}$ conformation.

An advantage of this mechanism is that it provides a discreet kinetic and thermodynamic model (Fig. 5) that can be tested by quantitatively fitting to a large body of electrophysiological data (22, 24). Based on the MD simulations, we expect conversions between the $Open_{out}$-$Closed_{in}$ and the $Closed_{out}$-$Open_{in}$ states to be rapid compared with the time scale of protonation/deprotonation. Thus, protonation shifts the equilibration population of states, rather than inducing an all-or-nothing transition. Our present MD simulations are not sufficiently accurate to determine the equilibrium constants defining the stability of the two states at various degrees of protonation. However, analysis of the conduction curves should allow extraction of the pertinent equilibrium and rate constants. For now, we assume a substantial population of both near the midpoint of the pH rate curve. Whereas a quantitative assessment of this model will be reported elsewhere, some qualitative features can be appreciated.

When $pH_{in}$ and $pH_{out}$ are matched, the inward and outward proton fluxes are equal, and no net current is observed. However, in an acidifying endosome, $pH_{out}$ decreases relative to $pH_{in}$ causing net inward flow of protons. The flow of a proton into the channel could easily occur via a proton wire leading to His-37 in the $Open_{out}$-$Closed_{in}$ state (Fig. 5). Protonation of His-37 would be followed by a rapid reequilibration between the $Open_{out}$-$Closed_{in}$ and $Closed_{out}$-$Open_{in}$ states. Deprotonation of His-37 and movement of a proton into the interior of the virus would be facilitated by the opening of the C-terminal pore in the $Closed_{out}$-$Open_{in}$ conformation. Once the proton reaches the interior of the virus, the channel would revert to its initial conformational ensemble, ready to enter a new cycle. Continuation of this process would favor inward flux until equilibrium is reached. This model predicts that the rate of channel conductance would saturate at low pH as the steady-state probability of

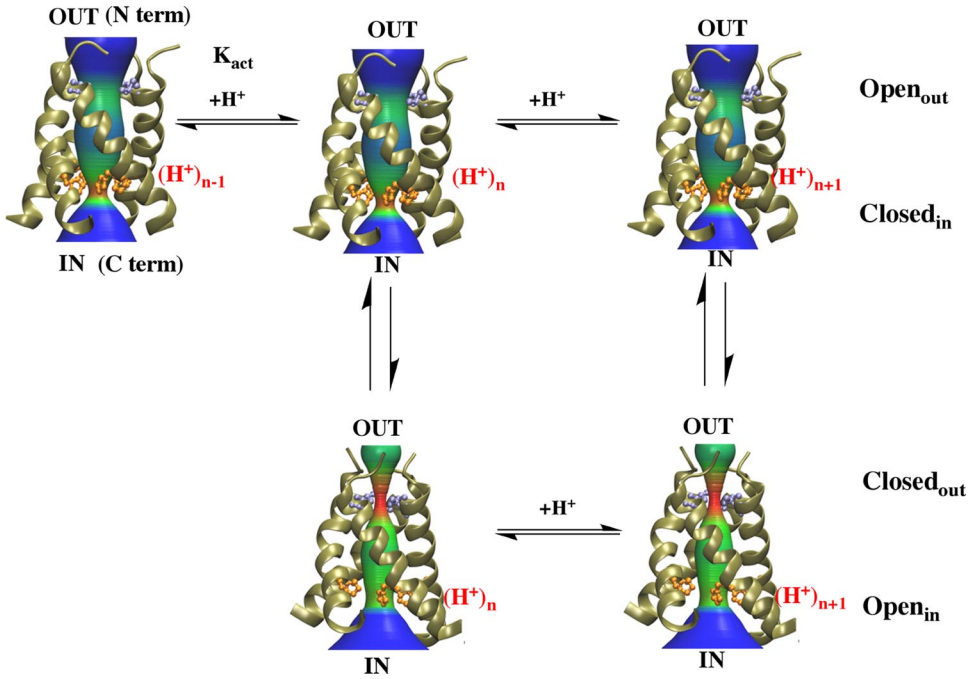


**Fig. 5.** M2 protein as proton transporter. Schematic mechanism of proton conduction through the M2. M2-TM exists in two conformational ensembles. In the $Open_{out}$-$Closed_{in}$ conformation the Val-27 gate is open and the His-37 gate is closed whereas the reverse is true for $Closed_{out}$-$Open_{in}$ conformation. At high $pH_{out}$, the $Open_{out}$-$Closed_{in}$ conformation is favored, because $pH_{out}$ decreases the His-37 residues get protonated and channel is activated at $K_{act}$ favoring the $Closed_{out}$-$Open_{in}$ conformation. Release of protons into the viral interior and deprotonation of His-37 stabilizes the $Open_{out}$-$Closed_{in}$ conformation and the cycle is repeated until equilibration.

finding the conducting His-37 sidechain in the protonated state approaches 1.0. At saturation, the magnitude of the proton flux would be limited by the rate of His-37 deprotonation, which is expected to occur on the ms time scale, matching the conductance of the channel (22).

This model also explains the asymmetric conductance observed for M2 from the UDORN and Weybridge strains of virus. These channels have low outward proton fluxes with low $pH_{in}$ and high $pH_{out}$ (e.g., $pH_{in}$ = 6.0, and $pH_{out}$ = 8.0) when compared with the opposite gradient ($pH_{in}$ = 6.0, and $pH_{out}$ = 8.0) (21, 24). Paradoxically, when the $pH_{out}$ is lowered to ≈6.5 to 7, significant outward currents are observed as long as the $pH_{in}$ is low (24). This led Chizmakov and coworkers to postulate an activation protonation with a $pK_a$ in this range, which we provisionally identify as $pK_{act}$ in Fig. 5. Note that high $pH_{out}$ is expected to strongly stabilize under-protonated states of the channel, which are not competent to conduct protons (far left in Fig. 5). Note, that in the under-protonated forms, the protein is expected to prefer the $Open_{out}$-$Closed_{in}$ conformation, in which His-37 is kinetically inaccessible to protons on the inside of the virus. Once the appropriate protonation state is reached, the outward flow of protons occurs by the inverse of the process observed for inward flow of protons.

Finally, this model is consistent with previous studies focusing on variants of the M2 proteins. Pinto *et al.* have shown that Trp-41 limits the accessibility of protons to His-37 from the inside of the virus (25). Changing this residue to other sidechains allows outward flow of protons under conditions of high $pH_{out}$-low $pH_{in}$ and/or an altered dependence of inward fluxes on $pH_{out}$. These findings are consistent with an increase in the exposure of His-37 to $pH_{in}$, and an alteration in its $pK_a$ associated with disruption of the His-37/Trp-41′ interactions in the $Open_{out}$-$Closed_{in}$ conformation. Chizmakov, Hay and coworkers have also noted that M2 from Rostock similarly allows outward flow of protons under conditions of high $pH_{out}$-low $pH_{in}$ (24). This protein has a substitution of Asp-44 for Asn, and introduction of the Asn44Asp mutation is sufficient to elicit the Weybridge phenotype. Interactions between Asp-44 and Arg-45 on a neighboring helix are critical to stabilizing the $Open_{out}$-$Closed_{in}$ conformation, and disruption of this interaction might be expected to alter the exposure of His-37 to $pH_{in}$ in this conformation.

## Conclusions

The simulations presented here provide support for the hypothesis that the protonation/deprotonation of His-37 occurs during the mechanism of proton conduction through M2, and suggest that the protein acts as a *proton transporter* with the His-37 gate closed as the Val-27 gate opens and vice versa. This mechanism does not require a single continuous wire of water molecules or ionizable groups spanning the entire protein. Instead, the present MD simulations suggest that the protein alternates between states with a low-energy path from the outside of the virus leading to His-37, and a second state connecting His-37 to the inside of the virus.

Furthermore, these structural and mechanistic insights are likely to be relevant for devising therapeutic strategies that use the M2 protein. Adamantane derivatives block the M2 activity and have been used for prophylaxis and treatment of influenza A infections (26), although the mode by which these drugs inhibit the function of M2 remains controversial (19, 20, 27). Sites of drug-resistant mutations line the region of the pore leading from the viral exterior to the His-37 gate [positions 26, 27, 30, 31, and 34] (28, 29). A recent mutational study supports the hypothesis that this region is a functionally important site to which the drug binds (30). Clearly, the presence of a large hydrophobic adamantyl group will largely impede the flow of protons through the pore leading to His-37, and may additionally alter the $pK_a$ of His-37, thereby upsetting the delicately balanced energetics of proton conduction (4, 20).

## Materials and Methods

**Simulation Details.** In all of the simulations, the protein structures were inserted in the transmembrane orientation into equilibrated and hydrated 1,2-dimyristoyl-sn-glycero-3-phosphocholine (DMPC) bilayer patch containing 64 lipids in each leaflet. The lipid and water molecules overlapping with the protein were removed. Sodium and chloride ions were added to the system at 150 mM concentration to maintain overall charge neutrality using 'Autoionize' plugin of VMD (31). Each system consisted of ≈24,000 atoms. MD simulations were performed using the code NAMD (32) with CHARMM22 protein force field (33), CHARMM27 lipid force field (34) and TIP3P water model (35). The temperature was maintained in all of the simulations at 310 K by coupling to a heat bath using the 'temperature coupling' method of NAMD. The energy minimizations of all of the systems were followed by equilibration runs. During the equilibration runs, first the heavy atoms of the protein were fixed for 1 ns; this was followed by 1 ns of harmonic constraints on the protein heavy atoms; followed by 1 ns of harmonic constraints on the $C_\alpha$ atoms. A force constant of 10 kcal/mol/Å was used for the harmonic constraints. These equilibration runs were followed by production runs of approximately 30 ns. During the first 2 ns of equilibration, a time step of 1 fs was used for the integration of the equations of motion. After 2 ns, a time step of 1.5 fs was used, with all of the hydrogen atoms constrained by using the SHAKE (36) and SETTLE (37) algorithms. Periodic boundary conditions were applied in three dimensions. The Langevin piston Nosé-Hoover method was used to maintain a pressure of 1 atm, allowing isotropic cell fluctuations. Nonbonded interactions were calculated every time step and full electrostatic interactions were calculated every two time steps. Long-range, electrostatics was taken into account via the particle mesh Ewald scheme (38, 39). The pore dimensions were computed using the HOLE program (40).

**ACKNOWLEDGMENTS.** We thank A. L. Stouffer for useful discussions and A. Kohlmeyer for enabling the computations. This work was supported by the National Institutes of Health and InfluMedix.

1. Lamb RA, Holsinger LJ, Pinto LH (1994) in *Receptor-Mediated Virus Entry into Cell*, ed Wimmer E (Cold Spring Harbor Laboratory Press, Cold Spring Harbor, NY), pp 303–321.
2. Salom D, Hill BR, Lear JD, DeGrado WF (2000) pH-dependent tetramerization and amantadine binding of the transmembrane helix of M2 from the influenza A virus. *Biochemistry* 39:14160–14170.
3. Nishimura K, Kim S, Zhang L, Cross TA (2002) The Closed State of a H+ Channel Helical Bundle Combining Precise Orientational and Distance Restraints from Solid State NMR. *Biochemistry* 41:13170–13177.
4. Hu J, *et al.* (2006) Histidines, heart of the hydrogen ion channel from influenza A virus: Toward an understanding of conductance and proton selectivity. *Proc Natl Acad Sci USA* 103:6865–6870.
5. Cady SD, Hong M (2008) Amantadine-induced conformational and dynamical changes of the influenza M2 transmembrane proton channel. *Proc Natl Acad Sci USA* 105:1483–1488.
6. Witter R, *et al.* (2008) Solid-state F-19 NMR spectroscopy reveals that Trp(41) participates in the gating mechanism of the M2 proton channel of influenza a virus. *J Am Chem Soc* 130:918–924.
7. Pinto LH, *et al.* (1997) A functionally defined model for the M-2 proton channel of influenza A virus suggests a mechanism for its ion selectivity. *Proc Natl Acad Sci USA* 94:11301–11306.
8. Wang J, Kim S, Kovacs F, Cross TA (2001) Structure of the transmembrane region of the M2 protein H+ channel. *Protein Sci* 10:2241–2250.
9. Cady SD, Goodman C, Tatko CD, DeGrado WF, Hong M (2007) Determining the Orientation of Uniaxially Rotating Membrane Proteins Using Unoriented Samples: A 2H, 13C, and 15N Solid-State NMR Investigation of the Dynamics and Orientation of a Transmembrane Helical Bundle. *J Am Chem Soc* 129:5719–5729.
10. Sansom MSP, Kerr ID, Smith GR, Son HS (1997) The influenza A virus M2 channel: A molecular modeling and simulation study. *Virology* 233:163–173.
11. Zhong QF, Newns DM, Pattnaik P, Lear JD, Klein ML (2000) Two possible conducting states of the influenza A virus M2 ion channel. *FEBS Letters* 473:195–198.
12. Zhong QF, *et al.* (1998) The M2 channel of influenza A virus: A molecular dynamics study. *FEBS Lett* 434:265–271.
13. Ayton GS, Voth GA (2007) Multiscale simulation of transmembrane proteins. *J Struct Biol* 157:570–578.
14. Kass I, Arkin IT (2005) How pH opens a $H^+$ channel: The gating mechanism of influenza A M2. *Structure* 13:1789–1798.
15. Chen HN, Wu YJ, Voth GA (2007) Proton transport Behavior through the influenza a M2 channel: Insights from molecular simulation. *Biophys J* 93:3470–3479.
16. Wu YJ, Voth GA (2005) A computational study of the closed and open states of the influenza A M2 proton channel. *Biophys J* 89:2402–2411.
17. Smondyrev AV, Voth GA (2002) Molecular Dynamics Simulation of Proton Transport through the Influenza A Virus M2 Channel. *Biophys J* 83:1987–1996.
18. Yi M, Cross TA, Zhou HX (2008) A secondary gate as a mechanism for inhibition of the M2 proton channel by amantadine. *J Phys Chem B* 112:7977–7979.
19. Schnell JR, Chou JJ (2008) Structure and mechanism of the M2 proton channel of influenza A virus. *Nature* 451:591–595.
20. Stouffer AL, *et al.* (2008) Structural basis for the function and inhibition of an influenza virus proton channel. *Nature* 451:596–599.
21. Pinto LH, Lamb RA (2006) Influenza virus proton channels. *Photochem Photobiol Sci* 5:629–632.
22. Mould JA, *et al.* (2000) Mechanism for proton conduction of the M-2 ion channel of influenza A virus. *J Biol Chem* 275:8592–8599.
23. Lin T-I, Schroeder C (2001) Definitive Assignment of Proton Selectivity and Attoampere Unitary Current to the M2 Ion Channel Protein of Influenza A Virus. *J Virol* 75:3647–3656.
24. Chizhmakov IV, *et al.* (2003) Differences in conductance of M2 proton channels of two influenza viruses at low and high pH. *J Physiol-London* 546:427–438.
25. Tang YJ, Zaitseva F, Lamb RA, Pinto LH (2002) The gate of the influenza virus M-2 proton channel is formed by a single tryptophan residue. *J Biol Chem* 277:39880–39886.
26. Kolocouris N, et al. (1996) Synthesis and antiviral activity evaluation of some new aminoadamantane derivatives. 2. *J Med Chem* 39:3307–3318.
27. Miller C (2008) Ion channels: Coughing up flu's proton channels. *Nature* 451:532–533.
28. Belshe RB, Smith MH, Hall CB, Betts R, Hay AJ (1988) Genetic-Basis of Resistance to Rimantadine Emerging During Treatment of Influenza-Virus Infection. *J Virol* 62:1508–1512.
29. Hay AJ, Zambon MC, Wolstenholme AJ, Skehel JJ, Smith MH (1986) Molecular-Basis of Resistance of Influenza-A Viruses to Amantadine. *J Antimicrob Chemother* 18:19–29.
30. Jing X, *et al.* (2008) Functional studies indicate amantadine binds to the pore of the influenza A virus M2 proton-selective ion channel. *Proc Natl Acad Sci USA* 105:10967–10972.
31. Humphrey W, Dalke A, Schulten K (1996) VMD- Visual Molecular Dynamics. *J Mol Graph* 14:33–38.
32. Phillips JC, *et al.* (2005) Scalable molecular dynamics with NAMD. *J Comput Chem* 26:1781–1802.
33. MacKerell AD, *et al.* (1998) All-Atom Empirical Potential for Molecular Modeling and Dynamics Studies of Proteins. *J Phys Chem B* 102:3586–3616.
34. Feller SE, Yin D, Pastor RW, MacKerell AD (1997) Molecular dynamics simulation of unsaturated lipid bilayers at low hydration: Parameterization and comparison with diffraction studies. *Biophys J* 73:2269–2279.
35. Jorgensen WL, Chandrasekhar J, Madura JD, Impey RW, Klein ML (1983) Comparison of simple potential functions for simulating liquid water. *J Chem Phys* 79:926–935.
36. Ryckaert JP, Ciccotti G, Berendson HJC (1977) Numerical integration of the cartesian equations of motion of a system with constraints: Molecular dynamics of *n*-alkanes. *J Comput Phys* 23:327–341.
37. Miyamoto S, Kollman PA (1992) SETTLE: An Analytical Version of the SHAKE and RATTLE Algorithm for Rigid Water Models. *J Comput Chem* 13:952–962.
38. Darden T, York D, Pedersen L (1993) Particle Mesh Ewald - an N. Log(N) Method for Ewald Sums in Large Systems. *J Chem Phys* 98:10089–10092.
39. Essmann U, et al. (1995) A Smooth Particle Mesh Ewald Method. *J Chem Phys* 103:8577–8593.
40. Smart OS, Goodfellow JM, Wallace BA (1993) The Pore Dimensions of Gramicidin A. *Biophys J* 65:2455–2460.